

# Implementing fluorescent MOFs as down-converting layers in hybrid light-emitting diodes

Enrico Angioni,<sup>a</sup> Ross J. Marshall,<sup>b</sup> Neil J. Findlay,<sup>b</sup> Jochen Bruckbauer,<sup>c</sup> Ben Breig,<sup>a</sup> David J. Wallis,<sup>de</sup> Robert W. Martin,<sup>c</sup> Ross S. Forgan<sup>b\*</sup> and Peter J. Skabara<sup>b\*</sup>

<sup>a</sup> WestCHEM, Department of Pure and Applied Chemistry, University of Strathclyde, G1 1XL, UK

<sup>b</sup> WestCHEM, School of Chemistry, University of Glasgow, Glasgow, G12 8QQ, UK

<sup>c</sup> Department of Physics, SUPA, University of Strathclyde, Glasgow, G4 0NG, UK

<sup>d</sup> Department of Materials Science and Metallurgy, University of Cambridge, Cambridge, CB3 0FS, UK

<sup>e</sup> Centre for High Frequency Engineering, University of Cardiff, Cardiff, CF24 3AA, UK

Email: [ross.forgan@glasgow.ac.uk](mailto:ross.forgan@glasgow.ac.uk) or [peter.skabara@glasgow.ac.uk](mailto:peter.skabara@glasgow.ac.uk)

## Abstract

One of the most important non-radiative relaxation processes that limits the quantum yield of a fluorophore is related to aggregation of the molecules in the solid-state causing excimer quenching. To limit this quenching mechanism, the fluorophore can be contained within a well-ordered 3D system that minimises aggregation through rigid bonds and spatial separation in a defined topological construct. Herein, the synthesis, characterisation and application as a down-converter of a new luminescent 3D material (**MOF-BTBMBA**) that incorporates a building block based on a benzothiadiazole (BT) derivative (**BTBMBA**) in a metal-organic framework (MOF) is presented. Notably, photoluminescent quantum yield and hybrid LED performance are significantly improved for the MOF-based device compared to that prepared with the free ligand, highlighting the effectiveness of the rigid scaffold arrangement.

## Introduction

Whilst organic light-emitting diodes (OLEDs) and inorganic light-emitting diodes (LEDs) have become ubiquitous as technologies underpinning display and lighting applications, hybrid inorganic/organic LEDs offer an alternative platform that combines the benefits of both material families.<sup>1-3</sup> For white light, these devices generally consist of a yellow emissive organic down-converting material on top of a blue-emitting inorganic LED and offer the

advantage of combining the well understood and high-performing electronic properties of inorganic LEDs with the broad, tuneable emission of organic semiconductors.<sup>4-6</sup> Furthermore, combining organic (or organic-based) materials with inorganic LEDs removes the need for traditional inorganic phosphor materials, such as cerium-doped yttrium aluminium garnet, reducing industry dependence on rare-earth materials as consumer demand increases.<sup>7</sup> Previously we have demonstrated a series of organic donor-acceptor molecular species that act as light-converting layers on top of inorganic InGaN-based LEDs.<sup>8-10</sup> We disclosed a blue-absorbing molecular colour-converter that incorporated an electron-deficient tetrafluorobenzene core into the fluorene-BODIPY scaffold. This molecule was designed to absorb in the blue and emit yellow light, providing an overall white emission when deposited on top of a blue LED.<sup>9, 10</sup> While this work provided the desired white light emission, device performance was compromised due to a lack of green light output, which is the wavelength region of the visible spectrum the human eye is most sensitive to, resulting in a lower than desired luminous efficacy and colour rendering index (CRI). An alternative family of molecules, based on the benzothiadiazole (BT) unit, was most recently reported, emitting more green light and hence offering improved luminous efficacy and colour rendering.<sup>11</sup> However, one remaining issue with these compounds is that, with increasing concentration, luminescence is quenched and the emission wavelength red-shifted due to aggregation of the molecules leading to non-radiative recombination.

To further address the detrimental effects of aggregation and therefore enhance efficiency, we sought to anchor a BT moiety in the confines of a metal-organic framework (MOF), a class of material where organic units are connected by metal ions or clusters into well-defined networks. BT units have a propensity to form  $\pi$ -stacked arrangements in the solid-state,<sup>12</sup> but the rigid topological construct of a network solid such as a MOF is expected to provide sufficient interspersing of the chromophore to preclude such aggregation and consequently improve the emissive properties, particularly the photoluminescence quantum yield, whilst maintaining the emission colour (Figure 1).<sup>13, 14</sup>

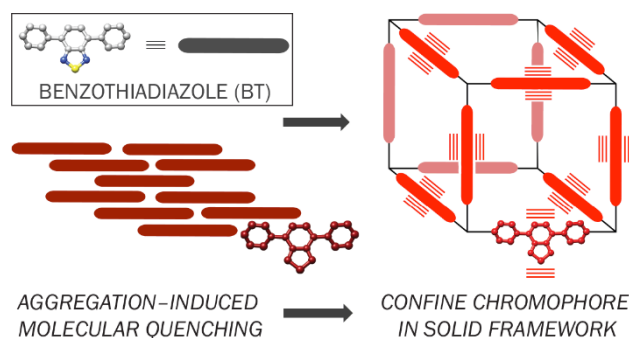


**Figure 1.** Schematic illustrating confinement of a benzothiadiazole chromophore in a network solid to avoid aggregation-based quenching mechanisms.

Organic and inorganic chromophores have previously been incorporated into the pores of MOFs as guests to prepare hybrid LEDs,<sup>15,16</sup> but utilising chromophores as integral components of the MOF scaffold should offer greater control over chromophore loading and spatial positioning. For example, Li and co-workers previously utilised a tetraphenylethylene-derived ligand with extended biphenyl arms (H<sub>4</sub>tcbpe, 4',4''',4''''',4''''''-(ethene-1,1,2,2-tetrayl)tetrakis ([1,10-biphenyl]-4-carboxylic acid) as the emissive component in the MOF Zn<sub>2</sub>(tcbpe). $\gamma$ DMA. The material could be suspension-processed onto commercially available blue LEDs to provide white light with a luminous efficacy of almost 60 lm W<sup>-1</sup>.<sup>17</sup> Herein, we have selected a Zr MOF<sup>18</sup> of the isorecticular UiO (Universitetet i Oslo) series, where Zr<sub>6</sub>O<sub>4</sub>(OH)<sub>4</sub> secondary building units (SBUs) connect linear dicarboxylate linkers, as the scaffold for chromophore incorporation, to take advantage of: (i) the rigid, well-spaced face-centred cubic (**fcu**) topology;<sup>19</sup> (ii) the anticipated excellent chemical and mechanical stability (we have previously shown that Zr MOFs with emissive 4,4'-[1,4-phenylene-bis(ethyne-2,1-diyl)]-dibenzoate linkers can act as luminescent water sensors);<sup>20,21</sup> (iii) the fine particle-size control available through modulated self-assembly.<sup>22</sup> We report the synthesis of a new emissive MOF (**MOF-BTBMBA**) containing a donor-acceptor-donor ligand and its application as a down-converting material on commercial blue LEDs. Notably, device inclusion of **MOF-BTBMBA**, as opposed to the free ligand (**BTBMBA**) alone, afforded an increased light output and conversion efficiency, suggesting that emissive MOFs containing donor-acceptor-donor ligands could find application as highly efficient optical materials.

## Results and Discussion

The final geometry of a MOF originates from the contribution of the metal's preferential coordination geometry and of the geometry of the ligand at the donating extensions;

following the principles of isorecticular synthesis, a well-defined SBU combined with rigid, linear ditopic ligands should result in a predictable topology. For this reason, and due to its linear conjugated backbone, the recently reported donor-acceptor-donor molecule dimethyl 4,4'-(benzo[*c*][1,2,5]thiadiazole-4,7-diyl)bis(3-methoxybenzoate)<sup>23</sup> was hydrolysed with an aqueous solution of sodium hydroxide and then acidified with hydrochloric acid to form the analogous dicarboxylic acid (**BTBMBA**) in 97% yield (Figure 2(a)). To examine the effect of its incorporation into a controlled solid matrix, it was decided to prepare a MOF linked by Zr that would be expected to exhibit a structure similar to UiO-68 (Figure 2(b)), which contains an unfunctionalised terphenyldicarboxylate linker and shows excellent stability.<sup>19</sup> Previously, related linkers containing central benzothiadiazole units flanked by two benzoic acid rings have been used to prepare Zr MOFs with UiO-68 topologies to sense picric acid<sup>24</sup> and organic amines,<sup>25</sup> or to photocatalytically degrade mustard gas simulants.<sup>26,27</sup> A selenothiadiazole analogue has also been utilised to photocatalyse dehydrogenative cross-coupling reactions.<sup>28</sup> In all but one case,<sup>25</sup> a mixed-linker synthetic strategy was used to prepare the MOF, where the photoactive ligand was diluted within the solid with an unsubstituted terphenyl analogue. Our own synthetic protocol used only the benzothiadiazole ligand for maximum loading of the photoactive units in the MOF, with hydrated zirconyl chloride as the Zr source and acetic acid as modulator to attempt to keep particle size low, which is expected to improve dispersion in the matrix used in device fabrication.

Powder-X-ray diffraction (PXRD) confirmed formation of the UiO-68 topology MOF with high crystallinity, with a close match to the pattern predicted from the crystal structure of the related PCN-56 (also described as UiO-68-Me<sub>4</sub>, CSD code YEYCOW)<sup>29</sup> material (Figure 2(c)). Pawley refinement of the room temperature powder diffraction data (See SI, Figure S5) gave a unit cell of  $a = 33.02947 \text{ \AA}$  in the  $Fm\bar{3}m$  space group, which strongly suggests **MOF-BTBMBA** has the expected UiO-68 topology. Scanning electron microscopy (Figure 2(d)) showed crystals of around 500-700 nm in size with characteristic octahedral morphology, and the MOF exhibited a moderate N<sub>2</sub> uptake at 77 K, with a Brunauer-Emmett-Teller (BET) surface area of 950 m<sup>2</sup> g<sup>-1</sup> (Figure 2(e)). This is lower than expected for a UiO-68 derivative,<sup>19</sup> and may be due to incomplete activation or a slight degradation in crystallinity during activation (heating to 120 °C under vacuum), observed by powder X-ray diffraction (PXRD) after the isotherm had been collected. Modifying the synthetic conditions to use L-proline as a modulator<sup>30,31</sup> resulted in yellow, octahedral single crystals, which unfortunately did not diffract strongly enough for a full structure solution, likely as a consequence of

rotation-induced disorder of the dissymmetric linkers. However, the F-centred cubic lattice ( $a = 32.5594(7)$  Å, likely  $Fm\bar{3}m$  space group, collected at 100 K) is again characteristic of a UiO-68 structure.<sup>22</sup>

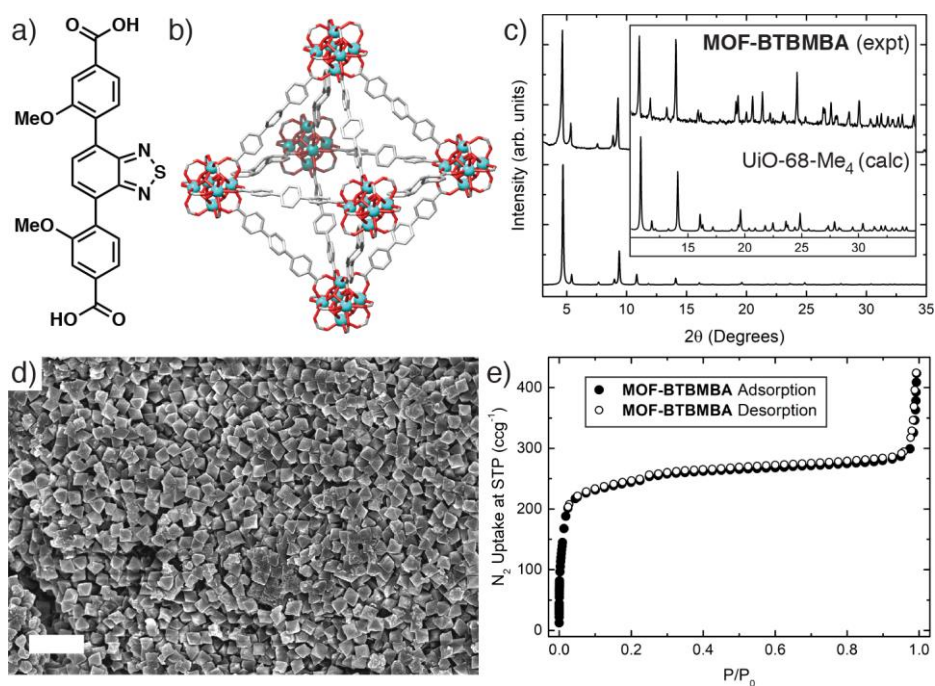


**Figure 2.** (a) Schematic structure of **MOF-BTBMBA**. (b) Representation of the crystal structure of UiO-68 showing the expected underlying topology of **MOF-BTBMBA**. (c) Powder X-ray diffraction pattern of **MOF-BTBMBA** compared to that predicted from the single crystal structure of the analogous UiO-68-Me<sub>4</sub> material (CSD code YEYCOW).<sup>29</sup> (d) Scanning electron micrograph of **MOF-BTBMBA** showing regular ~500 nm octahedral morphology (2 μm scale bar). (e) N<sub>2</sub> adsorption/desorption isotherm (77 K) for **MOF-BTBMBA**.

To measure the optical properties of **MOF-BTBMBA** and to have a fair comparison with the optical properties of the free ligand, both compounds were dispersed (1 mg ml<sup>-1</sup>) in the commercially available, optically clear polyurethane resin Opti-TEC™ 4200. This resin was chosen for its high transmittance (*ca.* 85%) across the visible electromagnetic spectrum of interest (350-700 nm) together with the possibility of obtaining a rigid encapsulation media after curing the resin by thermal treatment.<sup>32</sup> The absorption and emission band maxima show very similar behaviour, with absorption maxima at 408 and 412 nm, and emission maxima at 501 and 514 nm, for **MOF-BTBMBA** and **BTBMBA**, respectively (Figure 3). The slight blue-shift of both the absorption and emission maxima, together with the sharper bands for the MOF structure, can be attributed to the steric confinement of the ligand in **MOF-**

**BTBMBA** preventing aggregation that is likely observed in **BTBMBA** and resulting in a slightly altered local ligand environment.

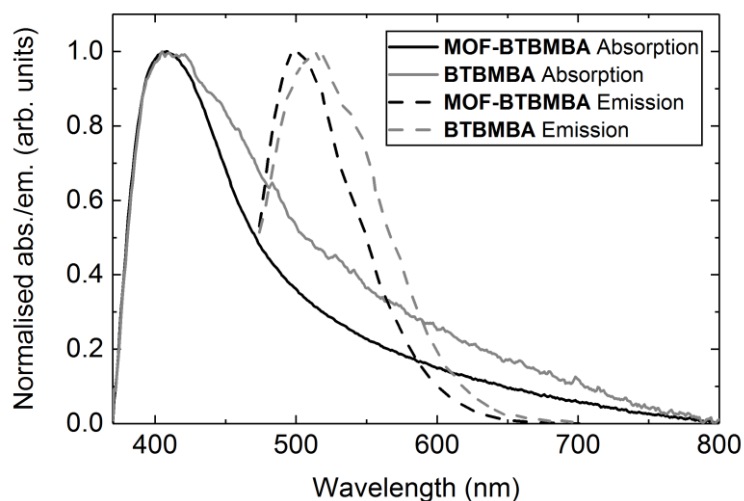


**Figure 3.** Absorption and emission spectra of ligand **BTBMBA** and **MOF-BTBMBA** when encapsulated as a film.

Photoluminescence quantum yields (PLQYs) were measured at 410 nm for the two materials dispersed in the OPT4200 resin ( $1 \text{ mg ml}^{-1}$ ), *via* drop casting 0.05 ml of each dispersion onto a quartz slide ( $1 \times 1 \text{ cm}$ ) and thermally curing the resin for 18 h at  $40 \text{ }^\circ\text{C}$ . Values of 42.5% and 2.3%, for **MOF-BTBMBA** and **BTBMBA**, respectively, indicate that inclusion of the ligand within the rigid MOF structure significantly increases the efficiency of the radiative emission process through restricting  $\pi$ - $\pi$  aggregation of the ligand in the solid state. As an approximation of emission efficiency using blue light as an excitation source, PLQYs were also measured at 445 nm. Values of 34.8% and 0.3% for **MOF-BTBMBA** and **BTBMBA**, respectively, were recorded, further evidencing the superior performance of the MOF compared to the free ligand.

For the fabrication of hybrid LEDs, a blue-emitting inorganic LED was coated with a transparent encapsulant containing either the ligand (**BTBMBA**) or the MOF (**MOF-BTBMBA**). The blue InGaN/GaN LEDs are based on the “GaN-on-Silicon” technology and emit at a wavelength of 453 nm. The encapsulant consists of a commercial polyurethane resin (Opti-TEC™ 4200) with hardener (1:1 ratio) into which either **BTBMBA** or **MOF-BTBMBA** is incorporated at different concentrations of 0.33 mg, 0.66 mg, 1 mg, 2 mg and 4 mg in 1 ml of encapsulant. The advantages of this type of encapsulant are high transparency, colour stability with respect to yellowing and flexibility after curing. After drop-casting the encapsulant mixture on top of the packaged LEDs they were cured at  $40 \text{ }^\circ\text{C}$  for 18 hours.

Figures 4(a) and (b) show the absolute electroluminescence (EL) spectra of the LEDs coated with the encapsulant containing the ligand and the MOF, respectively, for all concentrations (0.33-4 mg ml<sup>-1</sup>) measured at a constant forward current of 25 mA. In both sets of LEDs, the dominant emission peak around 450 nm corresponds to transmitted light from the blue LED, which is light that has not been absorbed by the organic material. Although weak, as evidenced by the logarithmic intensity scale, each set exhibits an additional longer wavelength emission (shoulder peak) around 550 nm. This can be associated with the emission from the encapsulated ligand and MOF material since it is not observed for the bare blue LEDs (solid dark blue lines in Figures 4(a) and (b)). Furthermore, the intensity of this longer wavelength emission peak increases with increasing concentration of the ligand/MOF in the transparent resin. Most notable, however, is that the intensity of this peak is much higher when the ligand is incorporated into a scaffold to form the MOF structure. This indicates that the rigid structure of **MOF-BTBMBA** is beneficial for enhanced light emission.

To further quantify the performance of the two materials, the luminous efficacy was determined for the ligand and MOF-coated LEDs as a function of concentration as displayed in Figure 4(c). The luminous efficacy is the ratio of the luminous flux and the electrical power supplied to the LED measured in lm/W. It describes the efficiency of converting electrical power into light taking the human eye response into account and is commonly used to describe white LEDs.<sup>9, 11</sup> For the LEDs coated with the ligand there is a decrease in luminous efficacy with increasing concentration, whereas the MOF-coated LEDs show an increase in efficacy. This trend is caused by the luminous flux since the electrical input power is roughly the same for all LEDs (see Figure 4(d)). This indicates that, in the absence of the MOF scaffold, the ligand absorbs the blue light but does not then re-emit it at longer wavelength as the concentration increases. In contrast, the opposite is true for the MOF structure. This quenching of the luminescence for the ligand is again most likely related to aggregation in the material, which is suppressed when the ligand is incorporated into the scaffold of the MOF structure. Furthermore, the radiant flux (Figure 4(e)) of both sets of LEDs decreases with increasing concentration, indicating that blue light is being absorbed for both sets of LEDs. In the case of the **BTBMBA** LEDs, the absorbed energy/light is lost non-radiatively, in contrast to the **MOF-BTBMBA** devices, where it is more efficiently down-converted.

To show the important effects of countering aggregation and to better compare both structures, the EL spectra of the bare blue LEDs and LEDs with the ligand or MOF at different concentrations were integrated in the same wavelength range of 525-600 nm, which corresponds to the emission range of the organic material. Figure 4(f) shows the ratio of the integrated intensity of the coated LEDs and the bare blue LEDs in this wavelength range. This ratio gives an indication of the increased emission for **MOF-BTB MBA** devices at a given concentration compared with the **BTB MBA** devices. With increasing concentration the ratio increases, and to a much greater extent for the MOF than the free ligand. At the highest concentration the emission from the **MOF-BTB MBA** device is approximately five times larger than the emission from the **BTB MBA** device.<sup>33</sup> This is also reflected by the previously mentioned PLQY, which is much higher for **MOF-BTB MBA** than **BTB MBA**. Again, this shows that firstly, the MOF is absorbing and re-emitting more of the light compared with the ligand alone and, secondly, that **BTB MBA** is quenching the luminescence. Overall, the emission of **MOF-BTB MBA** is larger compared to **BTB MBA**, showing the benefits of incorporating this ligand into the rigid MOF scaffold and therefore most likely reducing the detrimental quenching effects caused by the self-aggregation of the free ligand, **BTB MBA**.

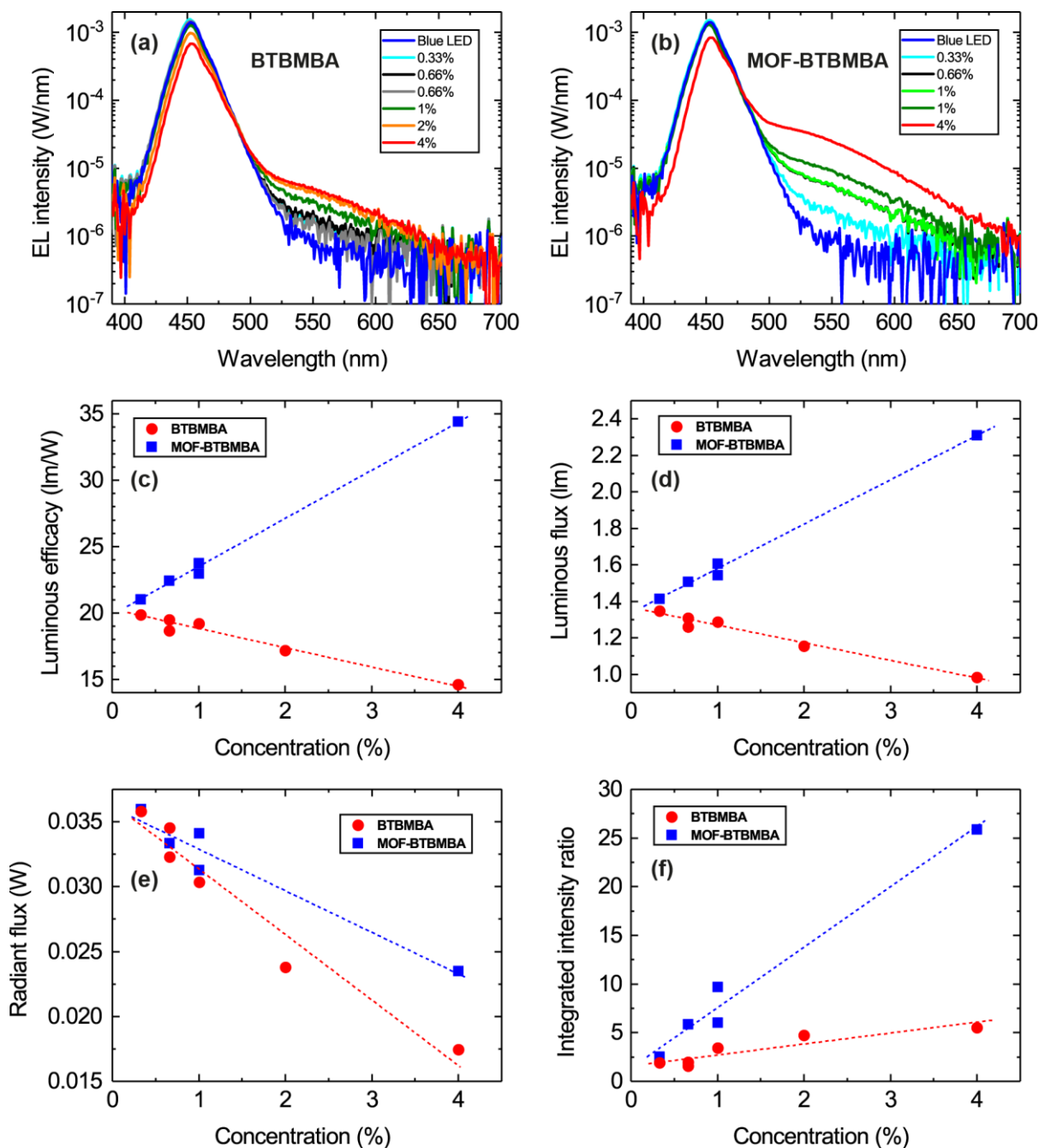


**Figure 4.** EL spectra of the blue LEDs coated with the (a) ligand **BTBMBA** and (b) **MOF-BTBMBA** using concentrations of 0.33-4%. The spectra, shown on a logarithmic scale, were recorded at a constant forward current of 25 mA. Please note that the scales for both graphs are the same. (c) Luminous efficacy, (d) luminous flux and (e) radiant flux of the ligand/MOF coated LEDs. (f) Ratio of the integrated intensities, in the wavelength range (525-600 nm), of the ligand/MOF coated LEDs and the blue LED. This corresponds to the spectral range of the emission from the organic material (ligand/MOF).

## Conclusion

We have detailed the synthesis of a novel and solution-processable emissive MOF material (**MOF-BTB MBA**) containing a donor-acceptor-donor ligand based on BT, and its application as a light-converting layer on top of a commercial blue LED. Notably, rigidification of the ligand within a solid-state scaffold significantly increases the PLQY (42.5% for **MOF-BTB MBA**, *c.f.* 2.3% for **BTB MBA** alone), counteracting aggregation and hence leading to improved device performance at low material loadings (~1-4% w/v) in a commercial polyurethane encapsulant, with intensity ratios (hybrid LED/blue LED) in the wavelength range of the organic emission five times greater for the MOF than the ligand alone. Hence, it is clear that the strategy of chromophore rigidification blocks aggregation and consequent non-radiative energy losses, suggesting that MOFs containing simple donor-acceptor-donor ligands have great potential as efficient down-converters for lighting applications.

## Acknowledgements

RSF thanks the Royal Society for a University Research Fellowship. EA, NJF and JB (EP/I012591/1, EP/N035496/1 and EP/P02744X/2) and RSF and RJM (EP/L004461/1) thank the EPSRC for funding. DJW acknowledges the support of EPSRC Manufacturing fellowship EP/N01202X/2. We acknowledge the EPSRC UK National Mass Spectrometry Facility (NMSF) at Swansea University for HRMS data, the EPSRC National Crystallographic Service for data collection,<sup>34</sup> Dr Claire Wilson, University of Glasgow, for preliminary crystallographic analysis, and Mr Dominic Bara, University of Glasgow, for PXRD fitting.

## Supporting Information

Characterisation data (NMR, HRMS, FTIR) for **BTB MBA** and **MOF-BTB MBA**, as well as Pawley fitting of the **MOF-BTB MBA** PXRD data, are detailed in the electronic supporting information file. The data underpinning this submission are available to download from <http://dx.doi.org/10.5525/gla.researchdata.662>.

## Experimental

Dimethyl 4,4'-(benzo[c][1,2,5]thiadiazole-4,7-diyl)bis(3-methoxybenzoate) was synthesised as described previously.<sup>21</sup> All reactions were performed using vacuum Schlenk lines, in an inert atmosphere of nitrogen or argon. Dry solvents were obtained from a solvent purification system (SPS 400 from Innovative Technologies) using alumina as the drying agent. MS

MALDI-TOF spectra were run on a Shimadzu Axima-CFR spectrometer (mass range 1-150000 Da). The high resolution mass measurements were performed on the Thermo Scientific LTQ ORBITRAP XL instrument. Thermogravimetric analyses (TGA) were performed using a Perkin-Elmer Thermogravimetric Analyser TGA7 under a constant flow of Argon ( $20 \text{ ml min}^{-1}$ ). The temperature was raised to  $50 \text{ }^\circ\text{C}$  followed by an isothermal period of 5 minutes. The temperature was raised again at a rate of  $10 \text{ }^\circ\text{C min}^{-1}$  until the desired temperature, at which point the material was left for an isothermal period of 30 minutes. The percentage weight loss over time was recorded at this temperature and the data was processed using the Pyris Series Software. Melting points were taken using a Stuart Scientific instrument SMP1. Differential scanning calorimetry was conducted on a TA Instruments DSC QC1000 with a RC-90 refrigerated cooling unit attached. The calibration was conducted using indium (melt temperature  $156.42 \text{ }^\circ\text{C}$ ,  $\Delta H_f 28.42 \text{ J g}^{-1}$ ). The test procedure used was a standard Heat-Cool- Reheat, which allows the removal of thermal history on the first heat allowing examination of any thermal processes on the cooling and second heat scan. The temperature range was from  $-50 \text{ }^\circ\text{C}$  to  $300 \text{ }^\circ\text{C}$  at  $10 \text{ }^\circ\text{C min}^{-1}$  unless otherwise stated. The electronic absorption spectra in the UV-Vis-NIR region were performed in solution using a Shimadzu UV 2700 spectrometer. The samples spectra were recorded against a white spectrum either in quartz cuvettes with 10 mm path length or in the solid state on quartz substrates. Luminescence emission spectra were recorded on a Perkin-Elmer LS45, on a Jasco FP-6500 or on an Edinburgh Instruments FLS980 spectrometer, either in solution in quartz cuvettes with 10 mm path length or in the solid state on quartz substrates. Infrared spectroscopy measurements were recorded as powder samples using a Shimadzu IRAffinity-1S spectrometer. Absolute PLQY measurements were performed in a calibrated integrating sphere attached to an Ocean Optics USB2000+ spectrometer, and a Gooch & Housego double monochromator with a quartz halogen lamp. The samples were excited at  $410 \text{ nm}$ .<sup>35</sup> PXRD measurements were carried out at  $298 \text{ K}$  using a PANalytical X'Pert PRO diffractometer ( $\lambda (\text{CuK}\alpha) = 1.4505 \text{ \AA}$ ) on a mounted bracket sample stage. Data were collected over the range  $2\theta = 5\text{--}45^\circ$ . Data were fit using GSAS-II.<sup>36</sup>  $\text{N}_2$  adsorption isotherms were carried out at  $77 \text{ K}$  on a Quantachrome Autosorb iQ gas sorption analyser. Samples were degassed under vacuum at  $120 \text{ }^\circ\text{C}$  for 20 hours using the internal turbo pump. BET surface areas were calculated from the isotherms using the Micropore BET Assistant in the Quantachrome ASiQwin operating software. Samples were imaged using a Carl Zeiss Sigma Variable Pressure Analytical SEM with Oxford Microanalysis, after coating with Pd for 150 seconds using Polaron SC7640 sputter coater. For the optical measurements of the blue LEDs

with and without the organic material applied the LEDs were placed inside a calibrated integrating sphere system (Labsphere illumina®plus 600/610). The recorded spectra, which were corrected for the system response, allow the determination of absolute intensity, such as the radiant and luminous flux, and hence the calculation of luminous efficacy. A Keithley 236 source measure unit was used for the constant current supply.

#### 4,4'-(Benzo[c][1,2,5]thiadiazole-4,7-diyl)bis(3-methoxybenzoic acid) BTBMBA

Dimethyl 4,4'-(benzo[c][1,2,5]thiadiazole-4,7-diyl)bis(3-methoxybenzoate) (0.385 g, 0.829 mmol) was dissolved in THF (150 ml) under nitrogen. Sodium hydroxide (2M aqueous, 14.9 ml, 29.8 mmol) was added and the mixture was heated to 75 °C for 20 h. After this time the obtained yellow suspension was dissolved in sodium hydroxide (2M aqueous solution, 100 ml) and the organic solvent was evaporated under reduced pressure. The resulting basic solution was acidified with concentrated hydrogen chloride until pH 1, stirred at room temperature for 1 h and then cooled (or stored) at -20 °C for 20 h. The mixture was filtered under reduced pressure, washed with water (3 × 50 ml) and dried under reduced pressure to obtain a yellow powder (350 mg, 0.802 mmol, 97%); <sup>1</sup>H NMR δ<sub>H</sub> (400 MHz, DMSO-*d*<sub>6</sub>): 13.16 (2H, s, COOH), 7.79 (2H, s, ArH), 7.72 – 7.68 (4H, m, ArH), 7.63 (2H, d, *J* = 8.1 Hz, ArH), 3.81 (6H, s, OCH<sub>3</sub>); <sup>13</sup>C NMR δ<sub>H</sub> (101 MHz, DMSO-*d*<sub>6</sub>): 167.1, 156.8, 153.3, 132.3, 131.7, 130.4, 130.0, 129.8, 121.5, 111.9, 55.7; *m/z* (%) (MALDI-TOF) 436.15 (90), 437.17 (100), 438.16 (60), 439.19 (15); HRMS (LSI-TOF) *m/z*: [M - H]<sup>-</sup> Calcd for C<sub>22</sub>H<sub>15</sub>N<sub>2</sub>O<sub>6</sub>S 435.0656; Found 435.0649; M.P.: 352-354 °C.

#### MOF-BTBMBA

BTBMBA (50 mg, 115 μmol) was suspended in DMF (10 ml) in a 25 ml screw top jar. ZrOCl<sub>2</sub>·8H<sub>2</sub>O (37 mg, 115 μmol) was added and the mixture sonicated. Acetic acid (0.5 ml, 525 mg, 8.7 mmol, 75 equiv) was added, and the mixture sonicated to yield a yellow solution. The mixture was sealed in the screw top jar and heated to 120 °C for 20 h. On cooling, the yellow powder was isolated by centrifugation, washed by suspension/centrifugation cycles with DMF (30 ml) and acetone (2 x 30 ml), and dried under vacuum to yield a yellow powder (51.5 mg, 82% based on Zr).

#### MOF-BTBMBA for single-crystal analysis

L-proline (54 mg, 0.47 mmol, 5 equiv) was dissolved in concentrated HCl (62.5 μL) and evaporated to dryness. The residue was dissolved in DMF (5 ml), and 1.25 ml of this solution

was added to a 25 ml screw top jar containing ZrCl<sub>4</sub> (22 mg, 95 μmol). To this, **BTBMBA** (41 mg, 95 μmol) and DMF (1.75 ml) were added and the mixture sonicated. The screw top jar was sealed and heated to 120 °C for 24 h. After cooling, the yellow octahedral crystals were examined by single crystal X-ray diffraction.

## References

1. P. Schlotter, R. Schmidt and J. Schneider, *Appl. Phys. A*, 1997, **64**, 417-418.
2. F. Hide, P. Kozodoy, S. P. DenBaars, A. J. Heeger, *Appl. Phys. Lett.*, 1997, **70**, 2664-2666.
3. C. Zhang and A. J. Heeger, *J. Appl. Phys.*, 1998, **84**, 1579-1582.
4. G. Heliotis, P. N. Stavrinou, D. D. C. Bradley, E. Gu, C. Griffin, C. W. Jeon, M. D. Dawson, *Appl. Phys. Lett.*, 2005, **87**, 103505.
5. E. Gu, H. X. Zhang, H. D. Sun, M. D. Dawson, A. R. Mackintosh, A. J. C. Kuehne, R. A. Pethrick, C. Belton, D. D. C. Bradley, *Appl. Phys. Lett.*, 2007, **90**, 031116.
6. V. M. Agranovich, Y. N. Gartstein and M. Litinskaya, *Chem. Rev.*, 2011, **111**, 5179-5214.
7. Z. Yue, Y. F. Cheung, H. W. Choi, Z. Zhao, B. Z. Tang and K. S. Wong, *Opt. Mater. Express*, 2013, **3**, 1906-1911.
8. N. J. Findlay, C. Orofino-Peña, J. Bruckbauer, S. E. T. Elmasly, S. Arumugam, A. R. Inigo, A. L. Kanibolotsky, R. W. Martin and P. J. Skabara, *J. Mater. Chem. C*, 2013, **1**, 2249-2256.
9. N. J. Findlay, J. Bruckbauer, A. R. Inigo, B. Breig, S. Arumugam, D. J. Wallis, R. W. Martin and P. J. Skabara, *Adv. Mater.*, 2014, **26**, 7290-7294.
10. J. Bruckbauer, C. Brasser, N. J. Findlay, P. R. Edwards, D. J. Wallis, P. J. Skabara and R. W. Martin, *J. Phys. D: Appl. Phys.*, 2016, **49**, 405103.
11. E. Taylor-Shaw, E. Angioni, N. J. Findlay, B. Breig, A. R. Inigo, J. Bruckbauer, D. J. Wallis, P. J. Skabara and R. W. Martin, *J. Mater. Chem. C*, 2016, **4**, 11499-11507.
12. S.-i. Kato, T. Matsumoto, T. Ishi-i, T. Thiemann, M. Shigeiwa, H. Gorohmaru, S. Maeda, Y. Yamashita and S. Mataka, *Chem. Commun.*, 2004, 2342-2343.
13. W. P. Lustig and J. Li, *Coord. Chem. Rev.*, 2018, **373**, 116-147.
14. T. N. Nguyen, F. M. Ebrahim and K. C. Stylianou, *Coord. Chem. Rev.*, 2018, **377**, 259-306.

15. C.-Y. Sun, X.-L. Wang, X. Zhang, C. Qin, P. Li, Z.-M. Su, D.-X. Zhu, G.-G. Shan, K.-Z. Shao, H. Wu and J. Li, *Nat. Commun.*, 2013, **4**, 2717.
16. Y. Cui, T. Song, J. Yu, Y. Yang, Z. Wang and G. Qian, *Adv. Funct. Mater.*, 2015, **25**, 4796-4802.
17. Z. Hu, G. Huang, W. P. Lustig, F. Wang, H. Wang, S. J. Teat, D. Banerjee, D. Zhang and J. Li, *Chem. Commun.*, 2015, **51**, 3045-3048.
18. Y. Bai, Y. Dou, L.-H. Xie, W. Rutledge, J.-R. Li and H.-C. Zhou, *Chem. Soc. Rev.*, 2016, **45**, 2327-2367.
19. J. H. Cavka, S. Jakobsen, U. Olsbye, N. Guillou, C. Lamberti, S. Bordiga and K. P. Lillerud, *J. Am. Chem. Soc.*, 2008, **130**, 13850-13851.
20. R. J. Marshall, Y. Kalinovsky, S. L. Griffin, C. Wilson, B. A. Blight and R. S. Forgan, *J. Am. Chem. Soc.*, 2017, **139**, 6253-6260.
21. C. L. Hobday, R. J. Marshall, C. F. Murphie, J. Sotelo, T. Richards, D. R. Allan, T. Düren, F.-X. Coudert, R. S. Forgan, C. A. Morrison, S. A. Moggach and T. D. Bennett, *Angew. Chem. Int. Ed.*, 2016, **55**, 2401-2405.
22. A. Schaate, P. Roy, A. Godt, J. Lippke, F. Waltz, M. Wiebcke and P. Behrens, *Chem. Eur. J.*, 2011, **17**, 6643-6651.
23. E. Angioni, M. Chapran, K. Ivaniuk, N. Kostiv, V. Cherpak, P. Stakhira, A. Lazauskas, S. Tamulevičius, D. Volyniuk, N. J. Findlay, T. Tuttle, J. V. Grazulevicius and P. J. Skabara, *J. Mater. Chem. C*, 2016, **4**, 3851-3856.
24. M. Sk and S. Biswas, *CrystEngComm*, 2016, **18**, 3104-3113.
25. W.-Q. Zhang, Q.-Y. Li, J.-Y. Cheng, K. Cheng, X. Yang, Y. Li, X. Zhao and X.-J. Wang, *ACS Appl. Mater. Interfaces*, 2017, **9**, 31352-31356.
26. S. Goswami, C. E. Miller, J. L. Logsdon, C. T. Buru, Y.-L. Wu, D. N. Bowman, T. Islamoglu, A. M. Asiri, C. J. Cramer, M. R. Wasielewski, J. T. Hupp and O. K. Farha, *ACS Appl. Mater. Interfaces*, 2017, **9**, 19535-19540.
27. W.-Q. Zhang, K. Cheng, H. Zhang, Q.-Y. Li, Z. Ma, Z. Wang, J. Sheng, Y. Li, X. Zhao and X.-J. Wang, *Inorg. Chem.*, 2018, **57**, 4230-4233.
28. W.-Q. Zhang, Q.-Y. Li, Q. Zhang, Y. Lu, H. Lu, W. Wang, X. Zhao and X.-J. Wang, *Inorg. Chem.*, 2016, **55**, 1005-1007.
29. H.-L. Jiang, D. Feng, T.-F. Liu, J.-R. Li and H.-C. Zhou, *J. Am. Chem. Soc.*, 2012, **134**, 14690-14693.
30. R. J. Marshall, C. L. Hobday, C. F. Murphie, S. L. Griffin, C. A. Morrison, S. A. Moggach and R. S. Forgan, *J. Mater. Chem. A*, 2016, **4**, 6955-6963.

31. O. V. Gutov, S. Molina, E. C. Escudero-Adán and A. Shafir, *Chem. Eur. J.*, 2016, **22**, 13582-13587.
32. Opti-TEC 4200 Optically Clear Polyurethane Encapsulant & Potting Compound, <https://www.intertronics.co.uk/product/opt4200-optically-clear-polyurethane-encapsulant-potting-compound/>).
33. The enhanced efficiency of **MOF-BTBMBA** occurs despite only 79% of the mass of the solid corresponding to the **BTBMBA** chromophore. As such, at 1 mg ml<sup>-1</sup>, the MOF-based device contains considerably less chromophore than the ligand-based device.
34. S. J. Coles and P. A. Gale, *Chem. Sci.*, 2012, **3**, 683-689.
35. J. C. de Mello, H. F. Whitmann and R. H. Friend, *Adv. Mater.*, 1997, **9**, 230-232.
36. B. H. Tony and R. B. Von Dreele, *J. Appl. Crystallogr.*, 2013, **46**, 544-549.